Joule

CellPress

Article

Stabilizing Solid Electrolyte-Anode Interface in Li-Metal Batteries by Boron Nitride-Based Nanocomposite Coating

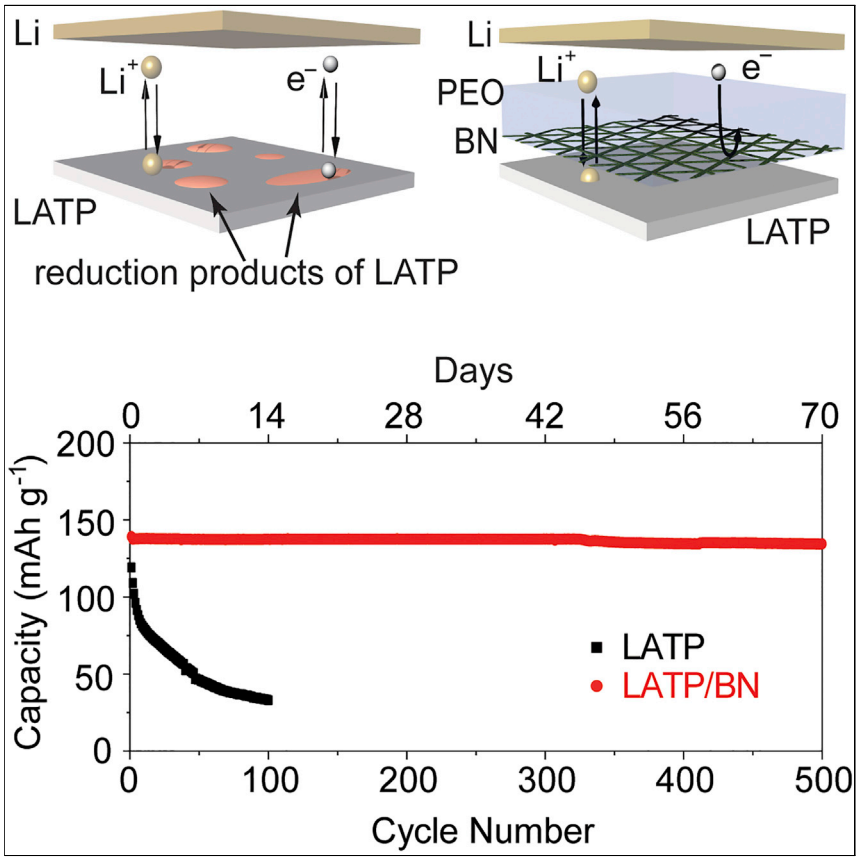

$Li_{1.3}Al_{0.3}Ti_{1.7}(PO_4)_3$ (LATP) solid electrolyte is inexpensive, light, and highly ionically conductive but unstable against Li metal. To avoid the side reactions between LATP and Li metal, chemically inert and mechanically robust BN nano-coating was deposited onto LATP solid electrolyte as a stable interface to enable stable cycling in Li-metal batteries. This strategy can be applied to various unstable solid electrolytes and extend lifetime of solid-state Li-metal batteries with high energy density.

Qian Cheng, Aijun Li, Na Li, ..., Dong Su, Kai Yan, Yuan Yang

pku.mckidd@gmail.com (K.Y.)
yy2664@columbia.edu (Y.Y.)

HIGHLIGHTS

Sub-10-nm thin BN film deposited by CVD effectively protects LATP against Li

In situ TEM analyzes the failure mechanism of LATP and the protective effect of BN

Solid-state batteries with LATP/BN show capacity retention of 96.6% over 500 cycles

Cheng et al., Joule 3, 1–13
June 19, 2019
https://doi.org/10.1016/j.joule.2019.03.022

Please cite this article in press as: Cheng et al., Stabilizing Solid Electrolyte-Anode Interface in Li-Metal Batteries by Boron Nitride-Based Nanocomposite Coating, Joule (2019), https://doi.org/10.1016/j.joule.2019.03.022

Joule

CellPress

Article

Stabilizing Solid Electrolyte-Anode Interface in Li-Metal Batteries by Boron Nitride-Based Nanocomposite Coating

Qian Cheng,[1,7] Aijun Li,[1,2,7] Na Li,[3,7] Shuang Li,[3] Amirali Zangiabadi,[1] Tai-De Li,[4] Wenlong Huang,[1] Alex Ceng Li,[1] Tianwei Jin,[1] Qingquan Song,[1] Weiheng Xu,[1] Nan Ni,[1] Haowei Zhai,[1] Martin Dontigny,[5] Karim Zaghib,[5] Xiuyun Chuan,[2] Dong Su,[3] Kai Yan,[6,*] and Yuan Yang[1,8,*]

SUMMARY

Solid-state Li-metal batteries are promising to improve both safety and energy density compared to conventional Li-ion batteries. However, various high-performance and low-cost solid electrolytes are incompatible with Li, which is indispensable for enhancing energy density. Here, we utilize a chemically inert and mechanically robust boron nitride (BN) film as the interfacial protection to preclude the reduction of $Li_{1.3}Al_{0.3}Ti_{1.7}(PO_4)_3$ (LATP) solid electrolyte by Li, which is validated by *in situ* transmission electron microscopy. When combined with ~1–2 μm PEO polymer electrolyte at the Li/BN interface, Li/Li symmetric cells show a cycle life of over 500 h at 0.3 mA·cm^{-2}. In contrast, the same configuration with bare LATP dies after 81 h. The $LiFePO_4$/LATP/BN/PEO/Li solid-state batteries show high capacity retention of 96.6% after 500 cycles. This study offers a general strategy to protect solid electrolytes that are unstable against Li and opens possibilities for adopting them in solid-state Li-metal batteries.

INTRODUCTION

Rechargeable solid-state Li batteries are promising candidates for next-generation energy storage, as solid electrolytes are much safer than conventional flammable organic electrolytes in Li-ion batteries.[1] The high modulus of solid electrolytes can help suppress Li dendrites, although Li growth along grain boundaries[2,3] and growth induced by electronic conduction[4] also need to be addressed. Therefore, solid electrolytes have the potential to improve the performance of Li batteries in terms of both safety and energy density.[5–9] Unfortunately, a wide range of solid-state electrolytes (SSEs) with high ionic conductivity can be reduced by metallic Li,[10,11] such as NASICON (e.g., $Li_{1.3}Al_{0.3}Ti_{1.7}(PO_4)_3$,[5,12] $Li_{1+x}Al_xGe_{2-x}(PO_4)_3$[13–15]), perovskite[16] (e.g., $Li_xLa_{2/3-x/3}TiO_3$,[17] thio-LISICON (e.g., $Li_{10}GeP_2S_{12}$,[18,19] $Li_{10}SnP_2S_{12}$[20]), and probably even garnet-type $Li_7La_3Zr_2O_{12}$ (LLZO).[19,21] To adopt these solid electrolytes in real applications, it is urgent to develop a chemically and mechanically stable interface, which is not only highly electronically insulating but also ionically conducting, to protect these solid electrolytes against the Li anode (Figures 1A and 1B).[4,22–24] Recently, significant efforts have been devoted to improving the stability of these solid electrolytes. For example, Ge film was demonstrated to protect $Li_{1+x}Al_xGe_{2-x}(PO_4)_3$ (LAGP), which allowed Li/LAGP/Li symmetric cells to cycle over 200 h at 0.3 mA cm^{-2} and Li-air batteries to cycle 30 times, but the impedance increased by more than 680% after 300 cycles.[14] Polymer coatings with a thickness of ~200 μm were also reported to stabilize

Context & Scale

Solid-state Li-metal batteries can improve safety and energy density compared to liquid-electrolyte-based Li-ion batteries; however, various ceramic electrolytes with high conductivities and low cost are not stable against Li metal, and the severe interfacial reaction devastates battery performance in several cycles. To stabilize the solid electrolyte-Li interface, we utilize boron-nitride-based nanocoating as the interfacial layer, which is not only electronically insulating and ionically conductive but also chemically and mechanically robust to preclude the reduction of solid electrolyte by the Li metal. With this strategy, $LiFePO_4$/LATP/BN/PEO/Li solid-state batteries show capacity retention of 96.6% over 500 cycles in 70 days. The development of boron-nitride-based protective film holds great potential to extend the electrochemical window of unstable solid electrolytes and expands the family of applicable solid electrolytes stable against Li metal.

Please cite this article in press as: Cheng et al., Stabilizing Solid Electrolyte-Anode Interface in Li-Metal Batteries by Boron Nitride-Based Nanocomposite Coating, Joule (2019), https://doi.org/10.1016/j.joule.2019.03.022

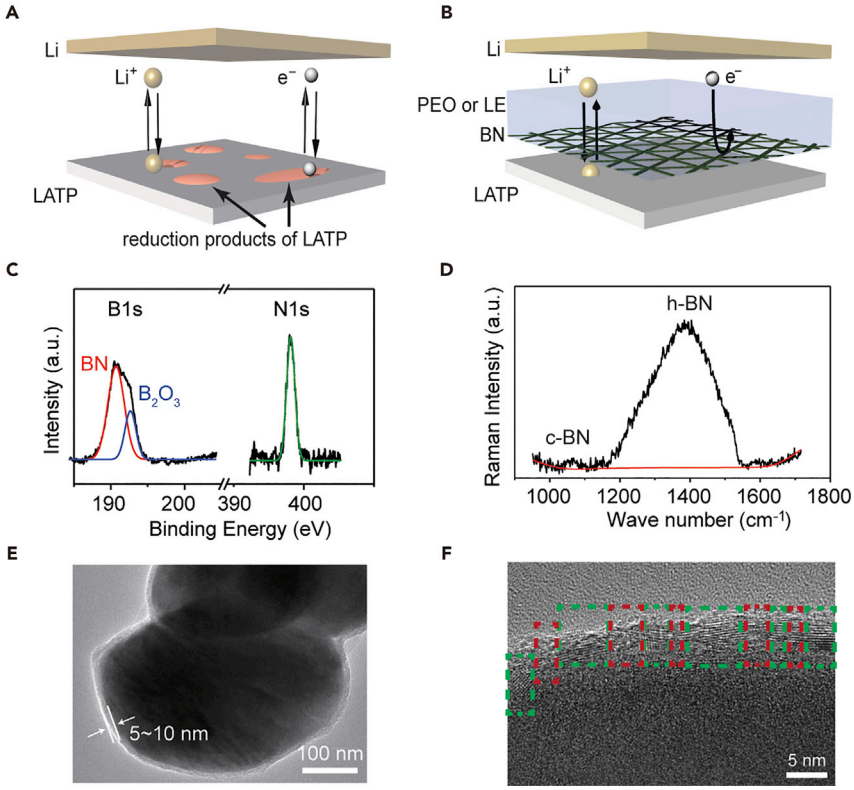

Figure 1. Schematics of the Protection Mechanism of BN and Characterizations of BN Nanofilm

(A) An LATP pellet that touches lithium metal will be immediately reduced. The interface in this scenario is composed of the reduction products of LATP, which are electronically and ionically conductive and thus incapable of stopping the continuous reduction of LATP.

(B) An artificial BN film is chemically and mechanically robust against lithium. It electronically isolates LATP from lithium but still provides stable ionic pathways when infiltrated by PEO or liquid electrolyte (LE).

(C) The XPS spectrum of BN, which was deposited onto the LATP pellet.

(D) The Raman spectrum of the BN protective layer.

(E) A TEM image of LATP/BN particles.

(F) A high-resolution TEM picture of the BN protective layer on the LATP particle. Green squares and red squares show crystalline regions and poorly crystalline or amorphous regions, respectively.

$Li_{1.3}Al_{0.3}Ti_{1.7}(PO_4)_3$ (LATP) with Li metal,[12] where the polymer layer can suppress Li dendrites depending on the magnitude of current density and exact mechanical properties.[2] However, the large thickness could lower the energy density of cells.

To address these challenges, we propose to use boron nitride (BN) nano-film as a protecting layer to isolate electrical contact between Li metal and the ionic conductor, along with a trace quantity of polymer or liquid electrolyte infiltrating the electrode-electrolyte interface, which is necessary to facilitate ion transport and reduce interfacial impedance (Figure 1B). BN is chosen as a protective layer since it is chemically and mechanically stable with Li metal.[25] It can be readily prepared by chemical vapor deposition (CVD) to form large-scale, atomically thin, and continuous films.[26,27] Unlike the thick polymeric protective layer (~200 μm) in previous reports,[12] such a thin film (~5–10 nm in this work) has a negligible effect on the energy density of Li batteries. BN also has a much lower electronic conductivity (10^{-15} S cm)[28] than common solid electrolytes (9.6×10^{-9} S cm^{-1} for LATP,[29] 10^{-8}–10^{-7} S cm^{-1} for LLZO, and 10^{-9}–10^{-8} S cm^{-1} for Li_2S–P_2S_5[4]), which

[1]Program of Materials Science and Engineering, Department of Applied Physics and Applied Mathematics, Columbia University, New York, NY 10027, USA

[2]Key Laboratory of Orogenic Belts and Crustal Evolution, School of Earth and Space Sciences, Peking University, Beijing 100871, China

[3]Brookhaven National Laboratory, Upton, NY 11973, USA

[4]Advanced Science Research Center in Graduate Center and Department of Physics at City College of New York, City University of New York, New York, NY 10031, USA

[5]Centre of Excellence in Transportation Electrification and Energy Storage (CETEES), Hydro-Québec, Varennes, QC J3X 1S1, Canada

[6]Amprius Inc., Sunnyvale, CA, USA

[7]These authors contributed equally

[8]Lead Contact

*Correspondence: pku.mckidd@gmail.com (K.Y.), yy2664@columbia.edu (Y.Y.)

https://doi.org/10.1016/j.joule.2019.03.022

Please cite this article in press as: Cheng et al., Stabilizing Solid Electrolyte-Anode Interface in Li-Metal Batteries by Boron Nitride-Based Nanocomposite Coating, Joule (2019), https://doi.org/10.1016/j.joule.2019.03.022

helps avoid dendrite growth induced by electronic conduction.[4] The Young modulus of the mono h-BN layer is approximately 1.0 TPa,[30] higher than ceramic electrolytes (81–115 GPa for LATP[31] and 150 GPa for c-LLZO[32]). Hence, mechanically, a conformal h-BN coating could also help suppress the growth of Li dendrites.[4] More importantly, the as-deposited BN layer has a mosaic structure with defects inside that allow Li ions to pass.[25] Therefore, the BN layer can provide excellent protection to SSEs without sacrificing the energy density of batteries. Yet, the addition of trace amount of polyethylene oxide (PEO) or liquid electrolyte is necessary to infiltrate the interface and enhance interfacial ion transport across the BN layer, which will be discussed in this manuscript.

We choose LATP as an example in this study, as it is inexpensive, highly conductive ($\sim$1 mS cm^{-1}),[33] and light ($\sim$2.9 g cm^{-3} versus 5.1 g cm^{-3} for LLZO).[31,34] However, it can be easily reduced at a high reduction potential of 2.17 V versus Li/Li^+.[10] The BN nano-coating layer can effectively protect LATP from reduction during Li plating and stripping, as validated by *in situ* transmission electron microscopy (TEM). Consequently, with the addition of 1–2 μm PEO at the interface, Li/BN/LATP/BN/Li symmetric cells show steady cycling over 500 h at 0.3 mA cm^{-2} and solid-state $LiFePO_4$/LATP/BN/Li battery shows capacity retention of 96.6% for 500 cycles in 70 days. The BN layer can also be combined with liquid electrolyte for high performance at room temperature, and stable cycling is achieved in both Li/Li cells (700 h at 0.5 mA cm^{-2}) and NMC/LATP/BN/Li cells (capacity retention of 93% in 100 cycles). These results demonstrate the effectiveness of BN coating to protect solid electrolytes against the high reducing power of Li metal.

RESULTS AND DISCUSSION

Synthesis and Characterizations of LATP/BN

LATP powders were synthesized by a sol-gel method modified from previous literature.[33,35] Stoichiometric amounts of lithium acetate and ammonium phosphate monobasic were dissolved in water, and aluminum nitrate and titanium butoxide were dissolved in ethanol. These two solutions were thoroughly mixed and dried to produce the gel precursor, which was calcined at 850°C to synthesize LATP powders. Then, the powders were pressed into pellets with a thickness of 0.5–1 mm and further annealed at 950°C to form dense, uniform, and highly crystalline LATP pellets (Figure S1A). The pellet has a high density of 2.66 g cm^{-3}, corresponding to 92% of its theoretical density. Such high density is crucial since the continuous deposition of BN can only be achieved on dense pellets to provide effective protection. Then, the boron nitride protective layer was deposited on the LATP pellet by CVD at 900°C with borane-ammonia complex (BH_3-NH_3) as the precursor in pure N_2.[27] Using 900°C, instead of a higher temperature, preserves the density of defective sites in the BN protective layer and thus yields better performance. After BN deposition, LATP pellets usually turn slightly blue (Figures S1D–S1F). Such a color change may originate from the formation of oxygen vacancies in the LATP during the BN deposition.[36] The scanning electron microscopy (SEM) image of LATP/BN pellet reveals a grainy and dense surface (Figure S2A), which is similar to that of bare LATP pellets (Figure S2B). The X-ray diffraction (XRD) patterns of both as-prepared LATP pellet and LATP/BN pellet match well with previous results ($LiTi_2[PO_4]_3$, JCPDS No. 35-0754),[37] validating that no change in crystal structure happens after BN deposition (Figure S2C).

To verify the successful deposition of BN, X-ray photoelectron spectroscopy (XPS) was applied to examine the existence of BN on the surface of LATP pellets (Figure 1C). The N 1s peak and the B 1s peak are clearly observed at the binding energy

Please cite this article in press as: Cheng et al., Stabilizing Solid Electrolyte-Anode Interface in Li-Metal Batteries by Boron Nitride-Based Nanocomposite Coating, Joule (2019), https://doi.org/10.1016/j.joule.2019.03.022

of 398.1 eV and 190.7 eV, respectively, both corresponding to the B-N bond.[38] The shoulder peak at 192.6 eV of the B 1s spectrum indicates the existence of B_2O_3, which is probably formed by the reaction between borane-ammonia complex and LATP.[39] Based on integrated peak area, the molar percentage of boron in B_2O_3 is 26%. The Raman spectrum (Figure 1D) shows that the BN film is mainly h-BN (1375 cm^{-1}) with a small amount of cubic BN (1,060 cm^{-1}).[40] The TEM image displays that LATP particles are uniformly coated by BN with a thickness of 5–10 nm (Figure 1E). The magnified high-resolution transmission electron microscopy (HRTEM) image illustrates that the BN coating is polycrystalline and has a mosaic structure, where the lattice plane is clear but with different orientations (Figure 1F). The interlayer distance is ~3.1 Å, similar to the previous report.[41] Small amorphous regions are also observed. This suggests that the BN layer contains a high concentration of defects (e.g., grain boundaries), which could facilitate Li ions to better permeate the coating. The homogeneity of the BN coating is further supported by energy-dispersive X-ray spectroscopy (EDS) mapping in the scanning transmission electron microscope (STEM) mode (Figure S3), where N signal distributes uniformly over LATP particles. Electron energy loss spectroscopy (EELS) mapping also shows that B and N uniformly distribute on the surface of LATP particles, exhibiting a conformal coating (Figure S4).

Stability of BN Nano-coating against Reduction

After confirming the conformal coating of BN, we used both cyclic voltammetry (CV) and *in situ* TEM to investigate whether the nanoscale BN coating can avoid the reduction of LATP particles by Li. In CV tests, Li is used as the counter electrode and Au is sputtered onto LATP pellets with and without BN (see Figure S5 for more details). In bare LATP, the reduction reaction is observed at 2.2 V versus Li/Li^+, which is assigned to Ti^{3+}/Ti^{4+}. In contrast, BN-coated LATP is highly stable in the range of 0–4.5 V versus Li/Li^+, demonstrating no activity toward reduction.

To further study the BN protection at the nanoscale, LATP or LATP/BN particles were placed on a Cu grid and Li contacted with the grid with a voltage of 1 V applied. For a bare LATP particle (Figures 2A and 2B), the diffraction pattern of $Li_3Al_{0.3}Ti_{1.7}(PO_4)_3$ phase (JCPDS No. 40-0095) was observed after just 5 min (Figure S6), indicating the existence of the following intercalation reaction:

$$Li_{1.3}Al_{0.3}Ti_{1.7}(PO_4)_3 + 1.7Li^+ + 1.7e^- \rightarrow Li_3Al_{0.3}Ti_{1.7}(PO_4)_3 \quad \text{(Equation 1)}$$

Then, the diffraction spots fainted and gradually disappeared in 20 min (Video S1). These results show that when LATP is reduced by Li metal, the intercalation of Li ions happens first and Ti^{4+} is reduced to Ti^{3+},[42] and then $Li_3Al_{0.3}Ti_{1.7}(PO_4)_3$ is further reduced until it is fully amorphous (Figures 2C and 2D). If the reaction keeps going for 1 h, there are drastic volume changes that will finally lead to particle cracking (Figure S7). Control experiments show that the electron beam cannot amorphize the bare LATP particle (Figure S8), but the voltage bias can slightly amorphize the bare LATP particle after 1 h (Figure S9). This shows that the negative voltage is one of the driving forces for the amorphization but not enough to fully reduce the LATP particles without Li.

On the contrary, the LATP/BN particle (Figures 2E and 2F) shows no structural change when reacting with Li for 1 h (Video S2) since no $Li_3Al_{0.3}Ti_{1.7}(PO_4)_3$ phase appears and the diffraction pattern (DP) matches well with that of LATP during the whole reaction (Figures 2G and 2H). Some new spots in Figure 2G, which appear with the double plane spacing of the original LATP crystal, are most likely caused

Please cite this article in press as: Cheng et al., Stabilizing Solid Electrolyte-Anode Interface in Li-Metal Batteries by Boron Nitride-Based Nanocomposite Coating, Joule (2019), https://doi.org/10.1016/j.joule.2019.03.022

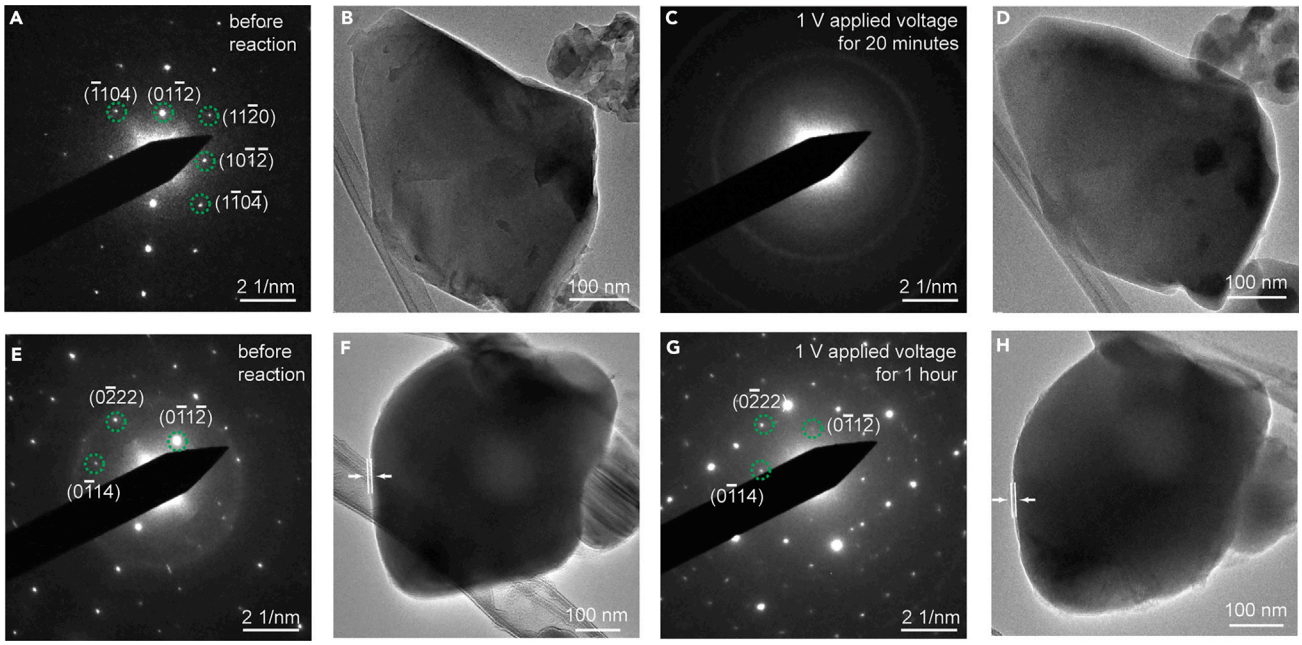

Figure 2. *In Situ* TEM Experiments to Study the Protective Effect of Nanoscale BN Coating

LATP particles and LATP/BN particles reacted with lithium under a potential of 1 V.

(A) The diffraction pattern and (B) the bright-field image of bare LATP particles before reacting with lithium.

(C) The diffraction pattern and (D) the bright-field image show that the particle turns completely amorphous after a 20-min reaction. The viewing direction is close to [2̄21̄].

(E) The diffraction pattern.

(F) The bright-field image of the LATP/BN particles before reacting with lithium.

(G) The diffraction pattern and (H) the bright-field image show that the particle and the protection film are intact after a 1 h reaction and the diffraction pattern still matches with LATP. The viewing direction of (E) and (G) is close to [100].

by the secondary diffraction or as a result of small deviation from the simulation of a perfect $LiTi_2(PO4)_3$ crystal (Figure S10).[43] These results strongly support that ~5–10 nm thin BN layer is enough to resist the reduction of LATP by Li.

The protection of BN is further validated at the macroscale by examining the color change of bare LATP and LATP/BN pellets in contact with Li. First, the bare LATP pellet turned black in 1 day after contacting dry Li metal (Figure S1B). This reduction process was dramatically accelerated with the addition of liquid electrolyte at the interface, as the LATP pellet turned black in just 5 min (Figure S1C). The reason is that the liquid electrolyte speeds up ion transport and hence the reduction reaction. In contrast, the LATP/BN pellet (Figure S1D) was stable with dry Li metal after 1 month (Figure S1E), even with the presence of the liquid electrolyte (Figure S1F), as the black spot rarely appeared on the LATP/BN pellet surface. Therefore, the BN coating allows the addition of liquid electrolyte to wet the electrode-electrolyte interface. Such benefit can efficiently resolve the long-standing challenge on Li-ion transport between the Li anode and the solid ceramic electrolyte and render cells with LATP or other unstable solid electrolytes operable at room temperature.[44]

Li/Li Symmetric Cells with LATP/BN Show Stable Li Plating and Stripping

In situ TEM, CV, and the color change tests demonstrate the high stability of the BN layer. Next, we examine the performance of the BN coating in electrochemical cells. First, bare LATP and LATP/BN pellets are examined with Au as the blocking electrodes to study the bulk conductivity. The conductivity of as-prepared dense LATP

Please cite this article in press as: Cheng et al., Stabilizing Solid Electrolyte-Anode Interface in Li-Metal Batteries by Boron Nitride-Based Nanocomposite Coating, Joule (2019), https://doi.org/10.1016/j.joule.2019.03.022

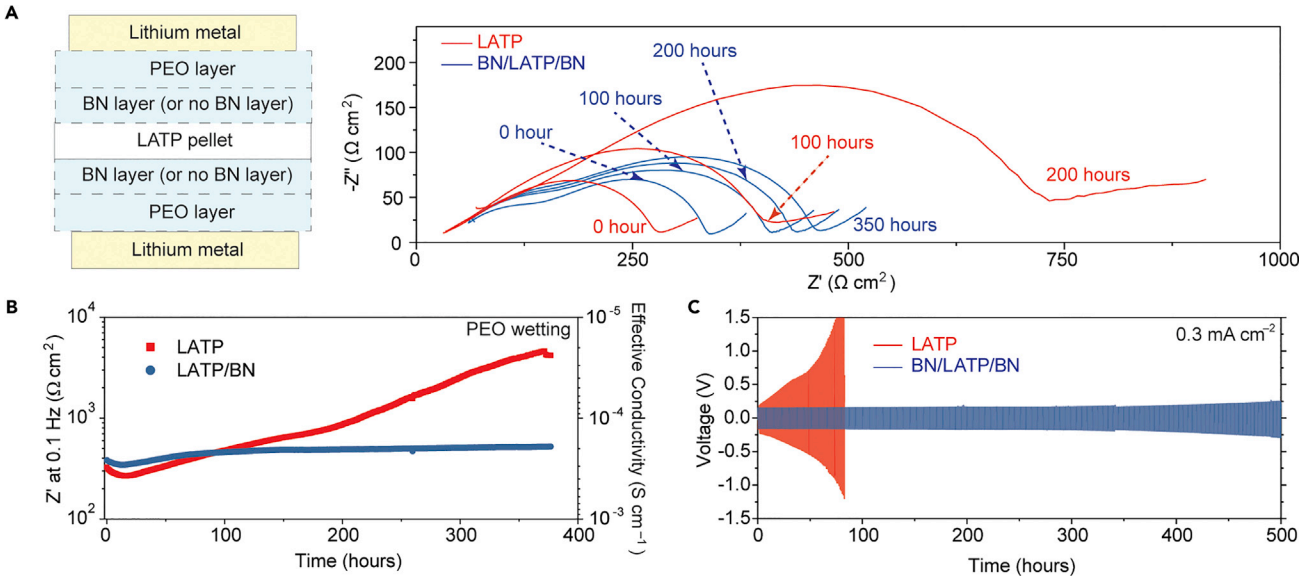

Figure 3. Electrochemical Characterizations of LATP and LATP/BN Pellets in Li/Li Symmetric Cells

(A) The schematic and the Nyquist plots of bare LATP and LATP/BN pellets in Li/Li symmetric cells with PEO infiltrating.

(B) The evolution of real impedance of Li/Li cells with bare LATP and LATP/BN pellets. 1–2 μm thick PEO was added on each side to wet the interface.

(C) The long-term cycling of Li/Li symmetric cells with bare LATP (red) and LATP/BN (blue) were tested at current density of 0.3 mA cm^{-2} and 60°C.

pellets reaches 2.0 × 10^{-4} S cm^{-1} at room temperature, similar to previous reports[31,33,45] (Figure S11A). For the LATP/BN pellet, an extra area specific resistance (ASR) of ~1600 Ω cm^2 is observed, which should be attributed to the BN layer, and the effective conductivity of the pellet is reduced to 4.7 × 10^{-5} S cm^{-1} (Figure S11B). Similar studies are also carried out in Li/Li cells. Li metal foils were pressed onto LATP at 50 MPa and electrochemical impedance spectroscopy (EIS) was measured at room temperature. The interfacial ASR of Li/BN/LATP/BN/Li cell is 3.0 × 10^4 Ω cm^2, which is much larger than that of the LATP/BN pellet. This should be attributed to the poor contact between Li and BN, as observed in other ceramic electrolytes (Figure S12; Table S1).[1] Although the ASR is large, it is very stable with BN coating. The overall ASR of Li/Li cells with BN coating only shows a 23% increase after 350 h (Figure S12A). In contrast, the EIS of cells with bare LATP increases dramatically from 1.9 × 10^4 Ω cm^2 at 0 h to 3.8 × 10^5 Ω cm^2 after 350 h (Figures S12B and S12C).

To realize stable interface and reduced interfacial resistance simultaneously, 1–2 μm thick PEO and lithium bis(trifluoromethylsulfonyl)imide (LiTFSI) polymer electrolyte with polyethylene glycol dimethyl ether as a plasticizer was added to infiltrate the interface (Figure 3A). The plasticity of PEO electrolyte can provide better contact and facilitate ion transport, while the chemical and mechanical stability of BN leads to excellent protection against Li. In previous studies, the ion-conductive polymer electrolyte layer typically has a thickness of 200 μm,[12] which eliminates direct contact between Li and LATP but dramatically lowers the energy density of the batteries. With the presence of BN film, the thickness of PEO can be reduced to 1–2 μm or even less since PEO is only used to accomplish better ionic contact between LATP and Li.

The impedance of Li/PEO/LATP/PEO/Li cells at 60°C (Figure 3A) can be fitted into two semicircles, which are (1) grain boundary resistance of LATP (R2) in parallel with constant phase element (CPE) for the inter-grain capacitance (Q2) and (2) charge transfer resistance (R3) in parallel with the CPE, which represents interfacial

Please cite this article in press as: Cheng et al., Stabilizing Solid Electrolyte-Anode Interface in Li-Metal Batteries by Boron Nitride-Based Nanocomposite Coating, Joule (2019), https://doi.org/10.1016/j.joule.2019.03.022

capacitance (Q3) at the electrolyte-Li interface. The two parallel circuits are in series with the bulk resistance of LATP (R1) (Figure S13A).[46] As we focus on how BN protects LATP against Li, which involves R1, R2, and R3, so the total resistance (R1 + R2 + R3) is used as the figure of merit for evaluating performance stability (Figure 3B).

The total resistance of Li/PEO/bare LATP/PEO/Li started at a low value of 286 Ω cm^2 with R2 of 182 Ω cm^2 and R3 of 85 Ω cm^2, indicating a low charge transfer resistance at the beginning (Table S2). This value (286 Ω cm^2) is much lower than the ASR of dry LATP pellets (Table S1) because the PEO electrolyte could diffuse into the bulk LATP pellet and reduce the interfacial impedance between domains. However, R2 and R3 grew quickly to 550 Ω cm^2 and 213 Ω cm^2 in 200 h and further climbed to 720 Ω cm^2 and 2,808 Ω cm^2 after 350 h (Figure S13C; Table S2), respectively. This result demonstrates that fast and adverse interfacial reactions deteriorate the charge transfer process and break the bonding of LATP grains during long-term contact. In contrast, the Li/PEO-BN/LATP/BN-PEO/Li cell exhibits a higher initial total ASR of 341 Ω cm^2. This primarily arises from a larger R3 of 157 Ω cm^2, which is likely because of the BN coating. Nevertheless, the BN coating remarkably enhances the stability of LATP and the solid electrolyte-Li interface: R2 and R3 only increase from 148 to 193 Ω cm^{-2} and from 157 to 241 Ω cm^2, respectively, after 350 h (Figure S13B; Table S2). In addition, the small thickness of PEO (1–2 μm) does not sacrifice the energy density of batteries (Figure S14).

After validating that the BN coating can stabilize the LATP-Li interface and the interfacial transport can be remarkably improved by the addition of PEO, the strength of this layer is further evaluated by galvanostatic cycling in Li/Li cells. The bare LATP cell with a current density of 0.3 mA cm^{-2} dies quickly within 81 h, while the cell with BN/LATP/BN pellet only shows a slightly higher overpotential from 156 mV at the beginning to 251 mV after 500 h (Figure 3C), demonstrating that the BN interface can yield stable Li plating and stripping.

Similar behavior is also observed in Li/Li cells when 2 μL liquid electrolyte of 1 M $LiPF_6$/EC/DEC is used to wet the BN layer. The edge of such cells was sealed by Kapton tapes to avoid bypassing of the liquid electrolyte (Figure S15). Without BN coating, the total ASR quickly increases from 146 to 1.3 $\times$ 10^5 Ω cm^2 in 400 h (Figure S16B). In contrast, the total ASR with BN coating only increased from 330 to 567 Ω cm^2, or 72%, after 400 h (Figure S16A). Further cycling of Li/Li cells at 0.1, 0.3, and 0.5 mA cm^{-2} all showed that cells with the bare LATP failed quickly, while the ones with LATP/BN only showed a slightly higher overpotential after 700 h cycling (Figures S16C–S16E). These results prove that the nanoscale BN coating can function effectively as a stable interface for LATP during Li stripping and plating.

BN Nano-coating Can Enable Long-Term Cycling of LATP with Li Metal in Full Cells

The stable Li stripping and plating in cells with LATP/BN suggests long cycling life in full cells since LATP is known to be stable with commercial cathodes, such as $LiNi_{0.33}Mn_{0.33}Co_{0.33}O_2$ (NMC) and $LiFePO_4$ (LFP) (Table S3). NMC/LATP/BN/Li and NMC/LATP/Li cells were tested first with liquid electrolyte (1 M $LiPF_6$ in EC/DEC) filling voids in the NMC electrode at room temperature (Figure S17A). The mass loading is ~4 mg cm^{-2} and the current density is 0.3 mA cm^{-2}. At 0.5 C (1 C = 150 mA g^{-1}), the initial specific capacity is 142 mAh g^{-1} and remains at 132 mAh g^{-1} after 100 cycles, corresponding to a capacity retention of 92.9% (Figures 4A and 4B). Without BN protection, the overpotential drastically increases to ~1.0 V in 30 cycles and the specific capacity drops to 27 mAh g^{-1} (Figure 4C), as a result of the high impedance

Please cite this article in press as: Cheng et al., Stabilizing Solid Electrolyte-Anode Interface in Li-Metal Batteries by Boron Nitride-Based Nanocomposite Coating, Joule (2019), https://doi.org/10.1016/j.joule.2019.03.022

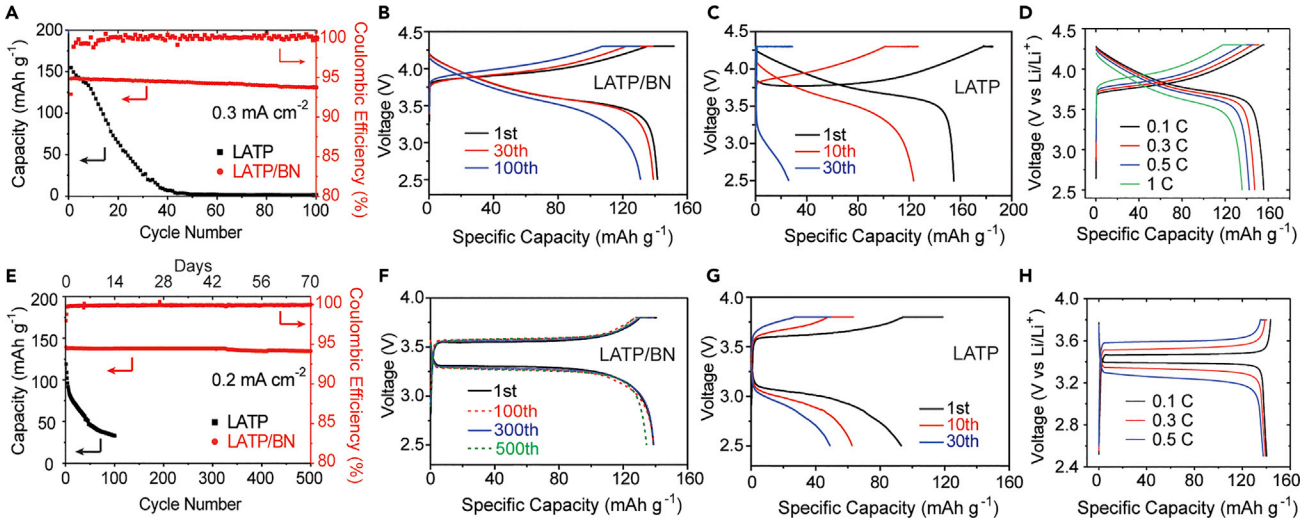

Figure 4. Electrochemical Characterizations of Full Cells Using LATP/BN or Bare LATP Pellet

(A) Cycling performance of NMC/LATP/Li cells with and without BN coating at a current density of 0.3 mA cm^{-2}. 2 μL liquid electrolyte was added on each side. The Coulombic efficiency is from the full cell with LATP/BN.

(B and C) Voltage profiles of NMC/LATP/Li cells (B) with BN coating and (C) without BN coating.

(D) The voltage profile of an NMC/LATP/Li cell at different rates.

(E) Cycling performance of LFP/PEO/LATP/PEO/Li cells with and without BN coating at a current density of 0.2 mA cm^{-2}. 1–2 μm PEO/LiTFSI (8:1) was applied on each side of the LATP pellet for infiltrating the interface. The operating temperature is 60°C.

(F and G) Voltage profiles of LFP/PEO/LATP/PEO/Li cells (F) with BN coating and (G) without BN coating.

(H) The voltage profile of an LFP/LATP/Li cell at different rates.

at the LATP/Li interface. This was further substantiated by the SEM images of LATP with and without BN coating. The bare LATP pellet shows high density of scrapes and cracks after 100 cycles (Figure S18A), which is not observed in LATP/BN (Figure S18B). This establishes BN-coated LATP as a viable approach for the stable Li stripping and plating and long-term operation in 4V NMC/Li rechargeable batteries. In addition, rate performance shows that the capacity retention is 86.5% at 1 C compared to that at 0.1 C, indicating reasonable power capability when the BN layer is wetted by the liquid electrolyte (Figures 4D and S19A).

To further demonstrate solid-state batteries with better thermal stability and safety, we also tried LFP/PEO/LATP/BN/PEO/Li cells with PEO/LiTFSI electrolyte infiltrated at both the BN layer and inside the LFP electrode (Figure S17B). The cathode loading is ~2.4 mg cm^{-2}. Then, the cell was tested at 60°C between 2.5 and 3.8 V. The initial discharge capacity of the LATP/BN cell reaches 139.2 mAh g^{-1} at 0.5 C (1 C = 170 mA g^{-1}) and remains at 134.5 mAh g^{-1} after 500 cycles (Figure 4E), and without notable increase in cell overpotential (Figure 4F). The average coulombic efficiency is as high as 99.9%. In contrast, the capacity of the cell without BN coating drops dramatically from the initial value of 119.1 mAh g^{-1} to 32.9 mAh g^{-1} after only 100 cycles. Such fast capacity decay is stimulated by the rapidly increasing overpotential (Figure 4G). Rate performance was also tested, and the capacity varies little with changing current density up to 0.5 C (Figures 4H and S19B).

To further understand the degradation mechanism of bare LATP, the LFP/Li cells are examined after cycling. Evidently, the bare LATP pellet was totally shattered after 100 cycles since 1–2 μm thin PEO is incapable of halting the reduction of LATP (Figure 5A). Cross-section and top-view SEM images further show that if the protection of BN is missing, the coarse surface and the formation of thick, reduced LATP

Please cite this article in press as: Cheng et al., Stabilizing Solid Electrolyte-Anode Interface in Li-Metal Batteries by Boron Nitride-Based Nanocomposite Coating, Joule (2019), https://doi.org/10.1016/j.joule.2019.03.022

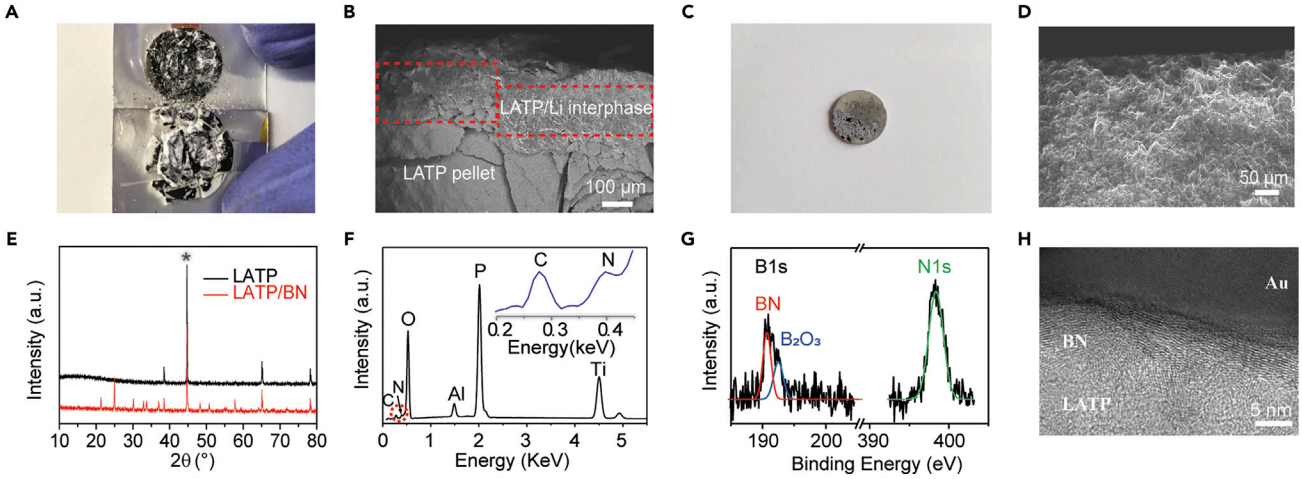

Figure 5. The Characterizations of Bare LATP Pellet and LATP/BN Pellet after Cycling in LFP/Li Solid-State Cells

(A) An optical image and (B) a cross-section SEM image of the bare LATP pellet. The bare LATP pellet was pulverized after 100 cycles and SEM shows that the reaction between LATP and lithium leads to a thick layer of reduced LATP and the stress induces the damage of the pellet.

(C) An optical image and (D) a cross-section SEM image of the LATP/BN pellet, which remained almost undamaged after 500 cycles.

(E) The XRD of bare LATP pellet after 100 cycles and LATP/BN pellet after 500 cycles. The peak * is from the Al stage of the instrument.

(F) The EDS spectrum.

(G) The XPS spectrum and (H) the HRTEM image of the LATP/BN pellet surface after 500 cycles, which show the durability of the BN nano-layer. The HRTEM sample is coated with Au first and then prepared by focused ion beam (FIB).

(~200–300 μm) are observed at the LATP/Li interface. These reduced products further propagate into the inside LATP pellet and introduce large internal stress and will eventually destroy the cell (Figures 5B and S18C). On the other hand, the LATP/BN pellet is intact after 500 cycles, with almost no sign of side reactions on the side-facing Li (Figure 5C). Both top-view (Figure S18D) and cross-section SEM pictures (Figure 5D) show that the surface of LATP/BN pellet still maintains in the well-fused state with high density, and no reduction product or cracks are formed at the interface or inside the LATP/BN pellet.

Further XRD characterization shows that the bare LATP pellet turns almost amorphous after 100 cycles, while the LATP/BN pellet maintains the original crystal structure (Figure 5E). Moreover, the EDS spectrum (Figure 5F) and mapping (Figure S20) confirm the existence of N (0.392 keV) at the surface after 500 cycles, which demonstrates the integrity of the protective layer. Further XPS results show that the binding energy of neither B nor N changes after cycling in LATP/BN pellets (Figure 5G). Based on the accumulated area of each peak, the percentage of B_2O_3-like species in the BN layer is 41%, slightly higher than the original percentage of 26%. Therefore, the BN appears to be reasonably stable after extended cycling. XPS mapping also shows that 57% of Ti^{4+} is reduced to Ti^{3+} in bare LATP after 100 cycles. In contrast, with BN coating, 98% of Ti remains at Ti^{4+}, and the 2% Ti^{3+} may even arise from background noise (Figure S21). HRTEM image further reveals that the BN layer is still conformal and intact at the LATP/Li interface even after 500 cycles in LFP/Li cells (Figure 5H). These results illustrate that the existence of BN film can effectively shield the reduction by Li so that LATP can function properly in solid-state Li-metal batteries.

The results above clearly demonstrate the effectiveness of the BN layer to avoid side reactions between Li metal and LATP. It is interesting to compare the BN coating and simply a layer of separator. A separator can electronically and physically separate

Please cite this article in press as: Cheng et al., Stabilizing Solid Electrolyte-Anode Interface in Li-Metal Batteries by Boron Nitride-Based Nanocomposite Coating, Joule (2019), https://doi.org/10.1016/j.joule.2019.03.022

LATP and Li and thus enhance cycling lifetime. However, the separator is typically thicker than 10 μm because of processing and its purpose to be a shield against the penetration of Li dendrites. Such a thick separator will lower the volumetric energy density of batteries. Moreover, the porous nature of separator will lead to the uptake of too much electrolyte, which lowers the energy density and makes the cell less safe. On the other hand, the thickness of BN is only ~5–10 nm, which has negligible effects on the energy density, and only a trace quantity of electrolyte is required.

Finally, we performed ignition tests on LATP pellets infiltrated by PEO or liquid carbonate electrolyte. Although the addition of liquid electrolyte or PEO facilitates ion transport at the interface, it heightens concerns about whether safety is compromised, which must be further evaluated. The results show that they are nonflammable (Video S3), indicating that a trivial amount of liquid electrolyte (4 μL) or PEO (1–2 μm thin) addition will not jeopardize battery safety.

Conclusions

In closing, we have successfully deposited boron nitride nano-film by CVD onto LATP pellets as a protective layer with a thickness of ~5–10 nm. Such a thin BN layer is electronically insulating but still allows Li ions to permeate. Thus, it acts as a barrier layer to prevent the reduction of LATP by Li metal. It is compatible with PEO for safe solid-state lithium batteries or with carbonaceous liquid electrolyte for 4 V Li batteries. By deploying BN coating on LATP, Li/LATP/Li symmetric cells show steady cycling over long time. Moreover, solid-state batteries in the configuration of LFP/PEO/LATP/BN/PEO/Li are demonstrated without capacity fading over 500 cycles in 70 days. These results show that the chemically stable BN coating is a promising choice as a protective layer without lowering the energy density of batteries, which opens possibilities for solid electrolytes that are not stable against the Li-metal anode. Further optimization of BN coating layer and LATP solid electrolyte itself will further reduce the voltage polarization and increase the performance.

EXPERIMENTAL PROCEDURES

Synthesis of LATP Pellets

The LATP powders were synthesized via a sol-gel method. $CH_3COOLi \cdot 2H_2O$ (99%, Alfa Aesar), $NH_4H_2PO_4$ (≥ 98.5%, Sigma Aldrich), $Al(NO_3)_3 \cdot 9H_2O$ (98%, Alfa Aesar), and $Ti(C_4H_9O)_4$ (97%, Sigma Aldrich) were used as starting materials. Stoichiometric amounts of $Al(NO_3)_3 \cdot 9H_2O$ and $Ti(C_4H_9O)_4$ were dissolved in 10 mL ethanol and an addition of 40 mL de-ionized-water-based solution with appropriate amounts of $CH_3COOLi \cdot 2H_2O$ and $NH_4H_2PO_4$ to form a precipitate. The solution was stirred at room temperature for 2 h and then dried at 95°C for 24 h to produce the gel precursor, which was further calcined at 850°C for 2.5 h to synthesize the LATP powders. The resulting powders were ball-milled, pressed into pellets, and sintered at 950°C for 10 h.

Boron Nitride Deposition for LATP Pellets

Boron nitride was deposited onto LATP pellets by low-pressure chemical vapor deposition (LPCVD). BH_3-NH_3 (97%, Sigma Aldrich) and pure nitrogen were used as the precursor and the carrier gas, respectively. The BH_3-NH_3 powder was placed in a porcelain boat inside a small quartz tube to prevent it from flowing away by the gas flow. Then, the precursor was heated to 70°C to produce the BH_3-NH_3 precursor gas, which would decompose and deposit onto LATP pellets at 400°C and 20 mTorr. After depositing for 0.5 h, the temperature was increased to 900°C with a ramping rate of 5°C per min and kept for another 1 h. Finally, it was cooled to room

Please cite this article in press as: Cheng et al., Stabilizing Solid Electrolyte-Anode Interface in Li-Metal Batteries by Boron Nitride-Based Nanocomposite Coating, Joule (2019), https://doi.org/10.1016/j.joule.2019.03.022

temperature at 5°C per min. The pressure during the reaction was ~85–100 Torr, and the N_2 gas flow was around 1.5 sccm.

Material Characterizations

The crystal structure of pellets was recorded by a PANalytical XPert3 Powder XRD with Cu Kα radiation at a scan rate of 0.1°/s. The morphology of samples was characterized on SIGMA VP Zeiss SEM and FEI TALOS F200X TEM. Ti^{3+} and Ti^{4+} mappings were done by the XPS (VersaProbe II, Physical Electronics) with Al Kα X-rays, at a 45-degree measuring angle. The spot size is 9 μm. After the Ti 2p spectra were measured, the T^{4+} and T^{3+} peaks were de-convoluted and used to plot the spatial distribution maps. The spontaneous Raman spectra were acquired by a laser confocal Raman microscope (Xplora, Horiba Jobin Yvon) with a 532 nm diode laser.

In Situ TEM Characterization

Cross-sectional TEM samples (bare LATP and LATP with BN) were dispersed on a TEM half-grid with amorphous carbon. The *in situ* TEM observation of lithiation into the sample was conducted with a JEM-2100F transmission electron microscope (JEOL) at an acceleration voltage of 200 kV and a Nanofactory scanning tunneling microscope (STM) holder. The Li metal is coated onto a piezo-driven tungsten (W) probe, which acts as the counter electrode. During the *in situ* lithiation, a constant negative DC potential (−1 V) was applied to the specimen and the lithiation processes were captured by real-time imaging in TEM-SAED mode.

Battery Assembly

$LiNi_{0.33}Mn_{0.33}Co_{0.33}O_2$ (NMC) cathode was prepared by mixing NMC, carbon black, and polyvinylidene fluoride (PVDF) at a mass ratio of 8:1:1 in N-methyl-2-pyrrolidone (NMP) to form a slurry, which was then coated on an Al foil, followed by drying at 110°C. The $LiFePO_4$ cathode was prepared by mixing $LiFePO_4$, carbon black, PVdF, and LiTFSI in NMP at a mass ratio of 8:1:1:1. The following steps are the same as NMC. Pouch cells were used for all tests, which were assembled in an argon-filled glove box with both moisture and oxygen levels below 0.1 ppm. For the PEO addition in the LFP cells, the PEO-based electrolyte was prepared with 1:1 mass ratio of poly (ethylene oxide) (PEO, M_V: 600,000 g/mol) to polyethylene glycol dimethyl ether 500 (M_V: 530.65 g/mol). The molar ratio of EO to LiTFSI is 8:1, which are all dissolved in acetonitrile. The PEO and acetonitrile solution is casted onto LATP pellets and dried at 60°C inside the glovebox before using. The nominal thickness of PEO after casting is 10 μm, but this layer is pressed down to 1–2 μm in real cells (Figure S14).

Electrochemical Measurements

All EIS tests were conducted with a VMP3 multichannel potentiostat from Bio-Logic in a frequency range of 1 MHz to 0.1 Hz with a 10-mV amplitude. Galvanostatic cycling of Li/Li cells and NMC/Li cells at different current densities were conducted on a Wuhan Land battery tester at room temperature, while LFP/Li full cells were tested at 60°C.

SUPPLEMENTAL INFORMATION

Supplemental Information can be found online at https://doi.org/10.1016/j.joule.2019.03.022.

ACKNOWLEDGMENTS

Dr. Y. Yang acknowledges support from the Air Force Office of Scientific Research (FA9550-18-1-0410) and support from Research Corporation for Science Advancement under award no. 26293. The authors greatly appreciate the funding support

from the National Science Foundation MRSEC program through Columbia in the Center for Precision Assembly of Superstratic and Superatomic Solids (DMR-1420634). A.L. would like to acknowledge the financial support from the China Scholarship Council (No. 201706010086), and X.C. acknowledges the Natural Science Foundation of China (No. 51774016). Electron microscopy work used the resources of the Center for Functional Nanomaterials, which is a US DOE Office of Science Facility, at Brookhaven National Laboratory under Contract No. DE-SC0012704.

AUTHOR CONTRIBUTIONS

Q.C., A.L., and N.L. contributed equally to this work. Y.Y. and K.Y. conceived the concept and supervised the study. Q.C. and A.L. synthesized and characterize the material, tested the performance, analyzed the results, and wrote the paper. N.L. and A.Z. did the *in situ* TEM characterization and analysis. All authors have discussed the results and revised the draft.

DECLARATION OF INTERESTS

The authors declare no competing interests.

Received: November 4, 2018
Revised: February 25, 2019
Accepted: March 24, 2019
Published: April 22, 2019

REFERENCES

1. Fu, K.K., Gong, Y., Liu, B., Zhu, Y., Xu, S., Yao, Y., Luo, W., Wang, C., Lacey, S.D., Dai, J., et al. (2017). Toward garnet electrolyte–based Li metal batteries: an ultrathin, highly effective, artificial solid-state electrolyte/metallic Li interface. Sci. Adv. *3*, e1601659.

2. Tikekar, M.D., Choudhury, S., Tu, Z., and Archer, L.A. (2016). Design principles for electrolytes and interfaces for stable lithium-metal batteries. Nat. Energy *1*, 16114.

3. Porz, L., Swamy, T., Sheldon, B.W., Rettenwander, D., Frömling, T., Thaman, H.L., Berendts, S., Uecker, R., Carter, W.C., and Chiang, Y.M. (2017). Mechanism of lithium metal penetration through inorganic solid electrolytes. Adv. Energy Mater. *7*, 1701003.

4. Han, F., Westover, A.S., Yue, J., Fan, X., Wang, F., Chi, M., Leonard, D.N., Dudney, N.J., Wang, H., and Wang, C. (2019). High electronic conductivity as the origin of lithium dendrite formation within solid electrolytes. Nat. Energy *4*, 187–196.

5. Manthiram, A., Yu, X., and Wang, S. (2017). Lithium battery chemistries enabled by solid-state electrolytes. Nat. Rev. Mater. *2*, 16103.

6. Yao, P., Zhu, B., Zhai, H., Liao, X., Zhu, Y., Xu, W., Cheng, Q., Jayyosi, C., Li, Z., Zhu, J., et al. (2018). PVDF/Palygorskite nanowire composite electrolyte for 4 V rechargeable lithium batteries with high energy density. Nano Lett. *18*, 6113–6120.

7. Xu, L., Tang, S., Cheng, Y., Wang, K., Liang, J., Liu, C., Cao, Y.-C., Wei, F., and Mai, L. (2018). Interfaces in solid-state lithium batteries. Joule *2*, 1991–2015.

8. Cheng, Q., Wei, L., Liu, Z., Ni, N., Sang, Z., Zhu, B., Xu, W., Chen, M., Miao, Y., Chen, L.-Q., et al. (2018). Operando and three-dimensional visualization of anion depletion and lithium growth by stimulated Raman scattering microscopy. Nat. Commun. *9*, 2942.

9. Jiao, S., Zheng, J., Li, Q., Li, X., Engelhard, M.H., Cao, R., Zhang, J.-G., and Xu, W. (2018). Behavior of lithium metal anodes under various capacity utilization and high current density in lithium metal batteries. Joule *2*, 110–124.

10. Zhu, Y., He, X., and Mo, Y. (2015). Origin of outstanding stability in the lithium solid electrolyte materials: insights from thermodynamic analyses based on first-principles calculations. ACS Appl. Mater. Interfaces *7*, 23685–23693.

11. Richards, W.D., Miara, L.J., Wang, Y., Kim, J.C., and Ceder, G. (2016). Interface stability in solid-state batteries. Chem. Mater. *28*, 266–273.

12. Zhou, W., Wang, S., Li, Y., Xin, S., Manthiram, A., and Goodenough, J.B. (2016). Plating a dendrite-free lithium anode with a polymer/ceramic/polymer sandwich electrolyte. J. Am. Chem. Soc. *138*, 9385–9388.

13. Chung, H., and Kang, B. (2017). Mechanical and thermal failure induced by contact between a $Li_{1.5}Al_{0.5}Ge_{1.5}(PO_4)_3$ solid electrolyte and Li metal in an all solid-state Li cell. Chem. Mater. *29*, 8611–8619.

14. Liu, Y., Li, C., Li, B., Song, H., Cheng, Z., Chen, M., He, P., and Zhou, H. (2018). Germanium thin film protected lithium aluminum germanium phosphate for solid-state Li batteries. Adv. Energy Mater. *8*, 1702374.

15. Wang, X., Zhai, H., Qie, B., Cheng, Q., Li, A., Borovilas, J., Xu, B., Shi, C., Jin, T., Liao, X., et al. (2019). Rechargeable solid-state lithium metal batteries with vertically aligned ceramic nanoparticle/polymer composite electrolyte. Nano Energy *60*, 205–212.

16. Knauth, P. (2009). Inorganic solid Li ion conductors: an overview. Solid State Ion. *180*, 911–916.

17. Ong, S.P., Mo, Y., Richards, W.D., Miara, L., Lee, H.S., and Ceder, G. (2013). Phase stability, electrochemical stability and ionic conductivity of the $Li_{10\pm1}MP_2X_{12}$ (M= Ge, Si, Sn, Al or P, and X = O, S or Se) family of superionic conductors. Energy Environ. Sci. *6*, 148–156.

18. Kamaya, N., Homma, K., Yamakawa, Y., Hirayama, M., Kanno, R., Yonemura, M., Kamiyama, T., Kato, Y., Hama, S., Kawamoto, K., et al. (2011). A lithium superionic conductor. Nat. Mater. *10*, 682–686.

19. Han, F., Zhu, Y., He, X., Mo, Y., and Wang, C. (2016). Electrochemical stability of $Li_{10}GeP_2S_{12}$ and $Li_7La_3Zr_2O_{12}$ solid electrolytes. Adv. Energy Mater. *6*, 1501590.

20. Bron, P., Johansson, S., Zick, K., Schmedt auf der Günne, J., Dehnen, S., and Roling, B. (2013). Li10SnP2S12: an affordable lithium superionic conductor. J. Am. Chem. Soc. *135*, 15694–15697.

21. Ma, C., Cheng, Y., Yin, K., Luo, J., Sharafi, A., Sakamoto, J., Li, J., More, K.L., Dudney, N.J., and Chi, M. (2016). Interfacial stability of Li metal-solid electrolyte elucidated via *in situ* electron microscopy. Nano Lett. *16*, 7030–7036.

22. Chen, L., Li, Y., Li, S.-P., Fan, L.-Z., Nan, C.-W., and Goodenough, J.B. (2018). PEO/garnet composite electrolytes for solid-state lithium batteries: from "ceramic-in-polymer" to "polymer-in-ceramic". Nano Energy *46*, 176–184.

23. Chi, S.-S., Liu, Y., Zhao, N., Guo, X., Nan, C.-W., and Fan, L.-Z. (2019). Solid polymer electrolyte soft interface layer with 3D lithium anode for all-solid-state lithium batteries. Energy Storage Mater. *17*, 309–316.

24. Li, D., Chen, L., Wang, T., and Fan, L.-Z. (2018). 3D fiber-network-reinforced bicontinuous composite solid electrolyte for dendrite-free lithium metal batteries. ACS Appl. Mater. Interfaces *10*, 7069–7078.

25. Yan, K., Lee, H.-W., Gao, T., Zheng, G., Yao, H., Wang, H., Lu, Z., Zhou, Y., Liang, Z., Liu, Z., et al. (2014). Ultrathin two-dimensional atomic crystals as stable interfacial layer for improvement of lithium metal anode. Nano Lett. *14*, 6016–6022.

26. Wang, M., Jang, S.K., Jang, W.J., Kim, M., Park, S.Y., Kim, S.W., Kahng, S.J., Choi, J.Y., Ruoff, R.S., Song, Y.J., et al. (2013). A platform for large-scale graphene electronics–CVD growth of single-layer graphene on CVD-grown hexagonal boron nitride. Adv. Mater. *25*, 2746–2752.

27. Shi, Y., Hamsen, C., Jia, X., Kim, K.K., Reina, A., Hofmann, M., Hsu, A.L., Zhang, K., Li, H., Juang, Z.-Y., et al. (2010). Synthesis of few-layer hexagonal boron nitride thin film by chemical vapor deposition. Nano Lett. *10*, 4134–4139.

28. Steinborn, C., Herrmann, M., Keitel, U., Schönecker, A., Räthel, J., Rafaja, D., and Eichler, J. (2013). Correlation between microstructure and electrical resistivity of hexagonal boron nitride ceramics. J. Eur. Ceram. Soc. *33*, 1225–1235.

29. Zhao, E., Ma, F., Guo, Y., and Jin, Y. (2016). Stable LATP/LAGP double-layer solid electrolyte prepared via a simple dry-pressing method for solid-state lithium ion batteries. RSC Adv. *6*, 92579–92585.

30. Lee, C., Wei, X., Kysar, J.W., and Hone, J. (2008). Measurement of the elastic properties and intrinsic strength of monolayer graphene. Science *321*, 385–388.

31. Jackman, S.D., and Cutler, R.A. (2012). Effect of microcracking on ionic conductivity in LATP. J. Power Sources *218*, 65–72.

32. Yu, S., Schmidt, R.D., Garcia-Mendez, R., Herbert, E., Dudney, N.J., Wolfenstine, J.B., Sakamoto, J., and Siegel, D.J. (2016). Elastic properties of the solid electrolyte $Li_7La_3Zr_2O_{12}$ (LLZO). Chem. Mater. *28*, 197–206.

33. Duluard, S., Paillassa, A., Puech, L., Vinatier, P., Turq, V., Rozier, P., Lenormand, P., Taberna, P.-L., Simon, P., and Ansart, F. (2013). Lithium conducting solid electrolyte $Li_{1.3}Al_{0.3}Ti_{1.7}(PO_4)_3$ obtained via solution chemistry. J. Eur. Ceram. Soc. *33*, 1145–1153.

34. Ohta, S., Seki, J., Yagi, Y., Kihira, Y., Tani, T., and Asaoka, T. (2014). Co-sinterable lithium garnet-type oxide electrolyte with cathode for all-solid-state lithium ion battery. J. Power Sources *265*, 40–44.

35. Zhai, H., Xu, P., Ning, M., Cheng, Q., Mandal, J., and Yang, Y. (2017). A flexible solid composite electrolyte with vertically aligned and connected ion-conducting nanoparticles for lithium batteries. Nano Lett. *17*, 3182–3187.

36. Liu, L., Gao, F., Zhao, H., and Li, Y. (2013). Tailoring Cu valence and oxygen vacancy in Cu/TiO_2 catalysts for enhanced CO_2 photoreduction efficiency. Appl. Catal. B Environ. *134–135*, 349–358.

37. Morimoto, H., Awano, H., Terashima, J., Shindo, Y., Nakanishi, S., Ito, N., Ishikawa, K., and Tobishima, S.-i. (2013). Preparation of lithium ion conducting solid electrolyte of NASICON-type $Li_{1+x}Al_xTi_{2-x}(PO_4)_3$ (x=0.3) obtained by using the mechanochemical method and its application as surface modification materials of $LiCoO_2$ cathode for lithium cell. J. Power Sources *240*, 636–643.

38. Ci, L., Song, L., Jin, C., Jariwala, D., Wu, D., Li, Y., Srivastava, A., Wang, Z.F., Storr, K., Balicas, L., et al. (2010). Atomic layers of hybridized boron nitride and graphene domains. Nat. Mater. *9*, 430–435.

39. In, S., Orlov, A., Berg, R., García, F., Pedrosa-Jimenez, S., Tikhov, M.S., Wright, D.S., and Lambert, R.M. (2007). Effective visible light-activated B-doped and B, N-codoped TiO_2 photocatalysts. J. Am. Chem. Soc. *129*, 13790–13791.

40. Reich, S., Ferrari, A.C., Arenal, R., Loiseau, A., Bello, I., and Robertson, J. (2005). Resonant Raman scattering in cubic and hexagonal boron nitride. Phys. Rev. B *71*, 205201.

41. Kim, K.K., Hsu, A., Jia, X., Kim, S.M., Shi, Y., Hofmann, M., Nezich, D., Rodriguez-Nieva, J.F., Dresselhaus, M., Palacios, T., et al. (2012). Synthesis of monolayer hexagonal boron nitride on Cu foil using chemical vapor deposition. Nano Lett. *12*, 161–166.

42. Lang, B., Ziebarth, B., and Elsässer, C. (2015). Lithium ion conduction in $LiTi_2(PO_4)_3$ and related compounds based on the NASICON structure: a first-principles study. Chem. Mater. *27*, 5040–5048.

43. Boucher, F., Gaubicher, J., Cuisinier, M., Guyomard, D., and Moreau, P. (2014). Elucidation of the $Na_{2/3}FePO_4$ and $Li_{2/3}FePO_4$ intermediate superstructure revealing a pseudouniform ordering in 2D. J. Am. Chem. Soc. *136*, 9144–9157.

44. Han, X., Gong, Y., Fu, K.K., He, X., Hitz, G.T., Dai, J., Pearse, A., Liu, B., Wang, H., Rubloff, G., et al. (2017). Negating interfacial impedance in garnet-based solid-state Li metal batteries. Nat. Mater. *16*, 572–579.

45. Gao, Z., Sun, H., Fu, L., Ye, F., Zhang, Y., Luo, W., and Huang, Y. (2018). Promises, challenges, and recent progress of inorganic solid-state electrolytes for all-solid-state lithium batteries. Adv. Mater. *30*, 1705702.

46. Busche, M.R., Drossel, T., Leichtweiss, T., Weber, D.A., Falk, M., Schneider, M., Reich, M.-L., Sommer, H., Adelhelm, P., and Janek, J. (2016). Dynamic formation of a solid-liquid electrolyte interphase and its consequences for hybrid-battery concepts. Nat. Chem. *8*, 426–434.